Fragmentation scheme of C_{60}^{4+} ions produced in low-energy collisions of Ar^{8+} and C_{60}

L. Chen, J. Bernard, A. Denis, S. Martin, and J. Désesquelles
Laboratoire de Spectrométrie Ionique et Moléculaire, Université Lyon 1, UMR CNRS No. 5579, 43 Boulevard du 11 November 1918, 69622 Villeurbanne Cedex, France

(Received 5 June 1998)

Fragmentation schemes of C_{60}^{4+} fullerene ions produced by bombardment of Ar^{8+} ions at low energies ($v \simeq 0.24$ a.u.) have been investigated. By analyzing the time of flight of the fragments in coincidence with the outgoing projectiles and the ejected electrons, several dissociation channels have been identified that involve the loss of small neutral as well as charged fragments. The probability of each channel has been measured experimentally and compared to the calculation based on a theoretical model including a statistical description of the evaporation, and a simulation of the multistep cascade decay for sequential losses of low mass fragments. The initial energy of the C_{60}^{4+} ion and the dissociation energy of each channel have also been evaluated. [S1050-2947(99)06004-7]

PACS number(s): 36.40.Qv, 36.40.Wa, 34.70.+e

I. INTRODUCTION

The mechanisms of excitation, ionization and fragmentation of the C_{60} molecule have been intensively studied during the past few years. Experimental investigations include photon excitation [1–3], C_{60}^{r+}-atomic target collision [4], electron impact collision [5–9] and highly charged ion collision [10–16]. In the multiphoton excitation as well as in the high-energy large-impact-parameter collision between an ion and a C_{60} molecule, the dominant excitation mode is the collective excitation of the valence electrons in giant dipole plasmon resonance. The charge state of the parent ion C_{60}^{r+} is limited to 1, 2, or 3, because the multiplasmon excitation is necessary for a high-order multiple ionization [2,10]. Highly charged C_{60}^{r+} ions up to 7+ have been observed in electron impact collisions [5], which shows a high stability of the C_{60} cage for the Coulomb explosion. With a two-sector-field mass spectrometer, Märk and co-workers [5–9] studied several fragmentation mechanisms for metastable C_{60}^{r+} ions (lifetime $\tau > 10\,\mu s$) produced in electron impact ionization. A number of channels have been identified, such as the sequential loss of neutral C_2 units [8]; the sequential reaction of C_{60}^{4+}, involving the loss of C_2^+ followed by the loss of C_2 or C_2^+ units [9]; and the superasymmetrical spontaneous decay reactions: $C_{60}^{r+} \rightarrow C_{58}^{(r-1)+} + C_2^+$. The last mechanism has been interpreted by a multistep reaction sequence started by a unimolecular C_2 evaporation, and followed by a charge transfer process from the heavy ion to the small neutral fragment [6].

In slow ion collisions, three cases can be distinguished. For large impact parameters, the over barrier extraction of electrons is dominant. Electrons are gently removed from the C_{60} cluster, leaving the C_{60}^{r+} ion in a stable charge state with r up to 9 [12]. For small impact parameters, the projectiles pass through the C_{60} cage or in its vicinity leading to a catastrophic destruction of the fullerene cage [11] with emission of charged light fragments and of a large number of electrons [14]. Recently, our group reported on the experimental observation of frontal collisions between an Ar^{8+} ion and a C_{60} target by measuring the energy loss of the projectile and the increase in electron emission [15]. An intermediate case can be observed with a proper selection of collision systems and impact parameters. In Xe^{8+} ion and C_{60} target collisions at 56 keV, C_{60}^{r+} ($r = 3,4,5$) ions are produced in excited states which decay by emitting small neutral or charged fragments in less than 100 ns after the collision [16].

The dominant fragmentation mechanism for an excited C_{60}^+ ion is described as a sequential loss or an ''evaporation'' of C_2 units following a fast statistical distribution of the initial energy into a large number of internal degrees of freedom of the parent ion. The dissociation energy of the channel $C_m^+ \rightarrow C_{m-2}^+ + C_2$ has been evaluated for $m = 60,58\ldots$ [17,18]. However, for highly charged C_{60}^{r+} ions, no data are actually available to determine the dissociation energy for the so-called asymmetrical ''fission channels,'' where charged small fragments are dissociated from the parent ion. The challenge here is to try to answer a simple question: what is the fragmentation scheme of a multicharged C_{60}^{r+} ion with a given internal energy? Experimentally the main difficulty is to select the initial charge state of the parent ion. One possible method is the two-sector-field mass spectrometer [5–9]. It is unfortunately limited to studying preselected individual fission channels and is thus suitable for the metastable processes.

In this paper, we present measurements of the probability for each asymmetrical fragmentation channel of C_{60}^{4+} ion produced in Ar^{8+} ion and C_{60} target collisions at low energy (56 keV). The collision events that produce a parent ion C_{60}^{4+} are identified by the coincidence of the outgoing projectile Ar^{6+} and the two ejected electrons. In fact, in our previous experiments [16], we have shown that the abundance of high mass fragments such as C_{60-2n}^{3+} and C_{60-2n}^{4+} with $n = 1,2,3,4,5$, is maximal when two electrons are stabilized on the projectile. The obtained experimental results are compared to a calculation using a simple statistical evaporation model, the so-called RRK theory developed by Rice, Ramsperger, and Kassel [19,20], and a multistep cascade decay model. The initial energy of C_{60}^{4+} ion and the dissociation energies of the fission channels, $C_m^{4+} \rightarrow C_{m-2}^{3+} + C_2^+$ and $C_m^{4+} \rightarrow C_{m-4}^{3+} + C_4^+$ with $m = 60,58,56,54$, have been determined.

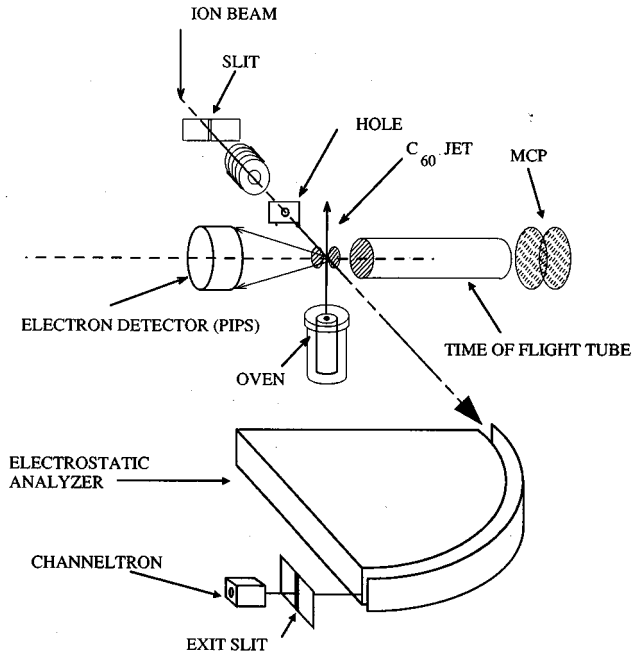

FIG. 1. Experimental setup. The scattered projectile ions are charge analyzed by a cylindrical electrostatic analyzer. The m/q ratio of the recoil ions is determined by their flight times in the TOF tube. The number of electrons ejected in a collision event is analyzed by a PIPS detector.

II. EXPERIMENT

The experimental setup is shown in Fig. 1. A 56-keV Ar^{8+} ion beam ($v \simeq 0.24$ a.u.) is delivered by a Nanogan 10-GHz electron cyclotron resonance (ECR) source and accelerated by a Danfysik accelerator. Its intensity is limited to a few tens of pA after collimation through a diaphragm of 500 μm. The ion beam crosses at a right angle an effusive fullerene molecular beam evaporated from an oven heated to 540 °C and containing a powder of about 99.9% of C_{60} and 0.1% of C_{70}. The outgoing projectiles are charge analyzed by a 90° cylindrical electrostatic analyzer ($R = 150$ mm) placed at 9.7 cm downstream of the collision zone. They are then detected by a channeltron electron multiplier ~600 ns after the collision. Electrons and recoil ions produced in the collision region are extracted by a transverse electric field of 100 V/mm. The electrons are accelerated through an intermediate electrode at a potential of 2500 V and collected several nanoseconds after the collision by a semiconductor detector [passivated implanted planar silicon detector (PIPS), 15-12-300] polarized at a high voltage of 20 kV. The signal from the PIPS is proportional to the total energy left by all the electrons arriving simultaneously. Thus it gives a measurement of the number of the electrons, since each electron carries almost the same energy of 20 keV. The signal is amplified and transmitted through an optical fiber in order to isolate the high-voltage dc component. The recoil ions, extracted in the opposite side, are post accelerated over a distance of 3 mm by an electric field of 1 kV/mm. After a field free drifting time in the time of flight (TOF) tube ($l = 149$ mm), they are detected by a multichannel plate multiplier. Pulses corresponding to the recoil ion fragments are sent to a multihit channel of a time to digital converter (TDC 3377, Le Croy) operated in common stop mode. The reference hit of the TDC is provided by the projectile signal with a delay of 6 μs. The same signal is also used as the trigger for an analogue to digital converter (ADC 811, Ortec) to analyze the electron signal that is suitably delayed. The mass to charge ratio m/q of an ion C_m^{q+} is determined by its time of flight. The time of flight of a fragment is different from that of its precursory ion if the fission is produced before the TOF tube. That limits the time range to observe the delayed fission of a C_{60}^{4+} ion to less than 250 ns in our experiment.

In a triple coincidence experiment, a collision event is identified by the simultaneous determination of the final charge state of the projectile ($8-s$ where s is the number of electrons stabilized on the projectile), the number of the emitted electrons and the TOF spectrum of the recoil ion fragments. In our experiments, the TOF spectra are recorded in different ways to get a detailed analysis of the fragmentation process. In a one-dimensional spectrum, the TOF is recorded in one of these ways: (1) only data related to the last detected fragment are taken; (2) data for all detected fragments are stored in a multistop spectrum; (3) the multistop spectrum is displayed according to the number of fragments, leading to one-stop, two-stop, three-stop, and four-stop spectra. In a two-dimensional spectrum, correlation information between fragments is analyzed.

III. RESULTS

Determination of the number of the electrons (n) emitted in a collision is crucial in our experiments. Because the initial charge state of the target C_{60}^{r+} is defined by n and the number of the electrons stabilized to the projectile s, $r = n + s$. Collisions producing a final Ar^{7+} projectile have been studied first. Figure 2 shows a two-dimensional scatter plot recorded in coincidence with outgoing Ar^{7+} projectiles. The electron signal is plotted along the Y axis and the time of flight of the corresponding last detected recoil ion along the X axis. The X-axis projection of this two-dimensional (2D) spectrum gives the TOF of the recoil ions. Only peaks corresponding to C_{60}^{r+} ions with $r = 1,2,3,4$ are observed. This is the evidence of the ''gentle collisions,'' which leave the targets charged and stable after collision with relatively large impact parameter. The Y-axis projections, related to recoil ions: C_{60}^{r+}, with $r = 2$, 3, and 4, show three spectra of electron multiplicity. For each spectrum, one notes a principal peak, which corresponds to the detection of n electrons such that the conservation of the total electron number, $r = s + n$ ($= 1 + n$ in this case), is verified. A secondary peak is observed between n and $n-1$, contributed by the backscattering of electrons in the PIPS detector [21]. In fact, the probability for an electron to release its total energy (20 keV) inside the detector is approximately 83%. In the remaining 17% cases, only a part of its energy, approximately 12 keV, is left inside the detector leading to the small low-energy peak. Taking this effect into account, we have calculated the electron energy distribution curves for the detection of one, two, and three electrons. The results are given by a solid line in each electron spectrum. The good agreement between the calculation and the experimental data allows us to estimate an efficiency of about 98% for electron detection in our experiments.

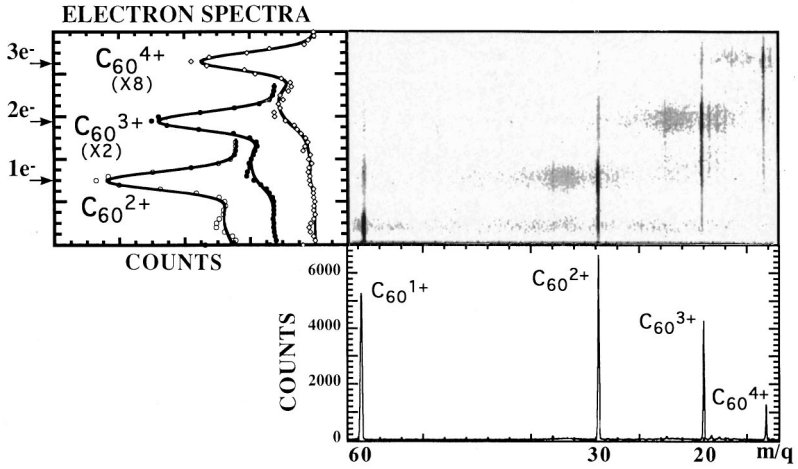

FIG. 2. Electron-recoil ion TOF 2D spectrum recorded in coincidence with Ar^{7+} ($s=1$). The pulse height of the electron detector is plotted in Y and the TOF of the last detected recoil ion of an event is plotted in X. The X axis is labeled in m/q where m is the number of carbon atoms of a fragment, q is the charge. The total X projection of the 2D spectrum shows stable C_{60}^{r+} peaks ($r=1$, 2, 3, and 4). Three Y projections associated with the detection of a well-defined recoil ion charge state C_{60}^{r+} ($r=2$, 3, and 4) present a principal electron number n peak at $n=1$, 2, and 3 electrons, respectively. The small peak between n and $n-1$ is due to the backscattered electron effect. The electron number conservation rule $r=s+n$ is verified.

Another 2D spectrum for the electrons and the TOF of the last detected recoil ion is shown in Fig. 3(a). It is recorded in coincidence with the detection of Ar^{6+} ($s=2$) outgoing projectiles. Three TOF spectra for the last detected recoil ion are obtained (Figs. 3(b)–(d)] from the X-axis projections associated to the detection of one, two, and three electrons. They correspond to collision events leading to charge states C_{60}^{3+}, C_{60}^{4+}, and C_{60}^{5+}, respectively. Remark that high-mass charged fragments are also observed in these spectra. The relatively intense C_{60-2n}^{3+} ($n=1,2,3,4,5$) peaks [Fig. 3(b)] show that the main decay channel for a C_{60}^{3+} parent ion is the evaporation of small neutral fragments. The asymmetrical fission channel is negligible here, because the corresponding peaks C_{60-2n}^{2+} ($n=1,2\ldots$) are very weak. C_{60-2n}^{3+} ($n=1,2\ldots$) peaks and C_{60-2n}^{4+} ($n=1,2\ldots$) peaks are observed with comparable intensities for a C_{60}^{4+} parent ion [Fig. 3(c)]. They correspond to the asymmetrical fission channels and the evaporation channels respectively. For a C_{60}^{5+} parent ion the evaporation channel is negligible. Only C_{60-2n}^{4+} and C_{60-2n}^{3+} high-mass peaks from one- and two-step asymmetrical fission are observed [Fig. 3(d)]. These results suggest that C_{60}^{r+} has a critical charge $r=4$ for which the evaporation and the fission channels become comparable. It is thus important to make a detailed study of the C_{60}^{4+} fragmentation scheme. Multifragmentation channels are demonstrated by the peaks of monocharged medium-mass ions C_m^+ with $m=6-15$ [Figs. 3(c) and 3(d)]. These peaks represent 20% and 50% of the population in the cases of the C_{60}^{4+} ion and the C_{60}^{5+} ion, respectively.

The TOF spectrum [Fig. 3(c)] is not sufficient to determine the fragmentation scheme of the parent ion C_{60}^{4+}, because each high-mass peak can correspond to one or several fission channels. For example, the C_{56}^{3+} peak could be attributed to four different channels: $C_{60}^{4+}\rightarrow C_{56}^{3+}+C_m^+ + C_{4-m}$ with m from 1 to 4. Further information can be obtained by studying the correlation between recoil ion fragments. The times of flight of charged fragments associated to a collision event are recorded in a 2D spectrum. The TOF of

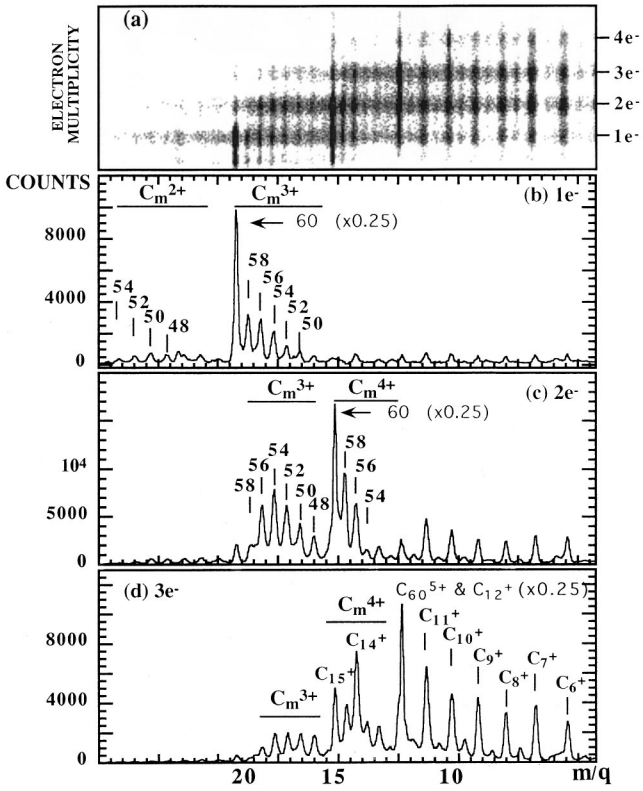

FIG. 3. (a) Electron-last detected recoil ion fragment TOF 2D spectrum registered in coincidence with Ar^{6+} ($s=2$). The X axis is labeled in m/q where m is the number of carbon atoms of a fragment and q is the charge. (b)–(d) The X projections of the 2D spectrum associated with the detection of $n=1$, 2, and 3 electrons give three TOF spectra produced by the dissociation of parent ions C_{60}^{3+}, C_{60}^{4+}, and C_{60}^{5+} ($s+n=r$), respectively. The C_{60}^{r+} peaks are reduced by a factor of 4.

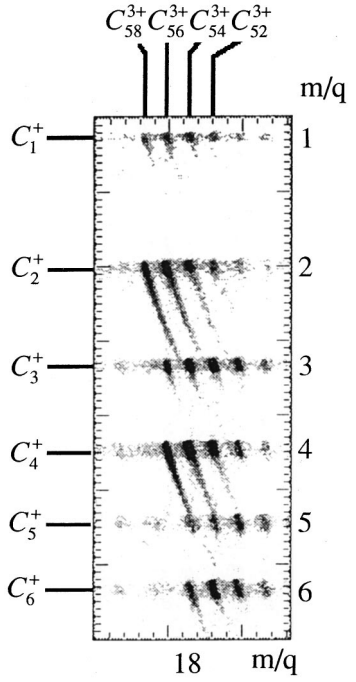

FIG. 4. Correlated recoil ion 2D spectrum produced by the dissociation of C_{60}^{4+} parent ion. The TOF of the last-detected fragment is plotted in *X* and the TOF of the other charged fragments of the same collision event are plotted in *Y*. Axes are labeled in m/q where m is the number of carbon atoms of a fragment and q is the charge.

the last detected fragment is plotted along the horizontal axis and that of other faster fragments along the vertical axis. Three similar 2D spectra have been simultaneously recorded in order to separate events corresponding to the detection of one, two, and three electrons. A fragment correlation spectrum for the C_{60}^{4+} parent ion is obtained (Fig. 4) when two ejected electrons are detected and after correction for the backscattered electron effect. Asymmetrical fission channels are represented by spots corresponding to the heavy fragments C_{58}^{3+}, $C_{56}^{3+}\cdots C_{52}^{3+}$ along the horizontal axis and to the light fragments C_1^+, $C_2^+\cdots C_6^+$ along the vertical axis. For example, the spot corresponding to the fragments C_2^+ and C_{58}^{3+} is related to the channel $C_{60}^{4+}\rightarrow C_2^+ + C_{58}^{3+}$. The spots related to the heavy fragment $m/q=18$ are actually due to C_{54}^{3+} and not to C_{18}^+, because no correlation has been observed between C_{19}^+ or C_{17}^+ and small fragments. Furthermore, the total 2D spectrum shows that the singly charged medium-mass fragments are correlated between them and that C_{18}^+ and C_{19}^+ have comparable intensities. The abundance for the fission channels is given by the intensities of the spots. They are shown in Table I and Fig. 5.

The abundance for the evaporation channels $C_{60}^{4+}\rightarrow C_{60-2n}^{4+}+$neutral fragments (Table I) is deduced from the intensities of the C_{60-2n}^{4+} peaks in Fig. 3(c) after correction. In fact, some of these peaks are also partially contributed by the medium-mass singly charged ion peaks C_m^+ ($m=13-19$) with the same or near m/q ratio. For example, the C_{52}^{4+} peak overlaps with the C_{13}^+ peak. The same situation occurs for C_{56}^{4+} and C_{14}^+, C_{60}^{4+} and C_{15}^+, C_{54}^{3+} and C_{18}^+. This effect is corrected as follows. Consider that the ions C_m^+ are produced from Coulomb explosion of a

TABLE I. Experimental abundance of the stable C_{60}^{4+}, the asymmetrical fission channels $C_{60}^{4+}\rightarrow C_m^+ + C_{60-2n}^{3+}$ ($m=1$ to 6), and the evaporation channels $C_{60}^{4+}\rightarrow C_2 + C_{60-2n}^{4+}$.

	C_{58}^{3+}	C_{56}^{3+}	C_{54}^{3+}	C_{52}^{3+}	C_{50}^{3+}	C_{48}^{3+}
C^+	650	1140	920	380	185	
C_2^+	5400	6510	3045	980	360	
C_3^+		1850	3400	3230	1890	
C_4^+		8190	8650	4640	1460	
C_5^+			770	910	1290	930
C_6^+			2150	3100	2040	685
	C_{58}^{4+}	C_{56}^{4+}	C_{54}^{4+}	C_{52}^{4+}		
C_2	19 860	8120	1720	450		
C_{60}^{4+}	102 300					

C_{60}^{4+} ion giving four charged fragments with equal detection probability *K*. The probability to detect *w* fragments among four in such an event is determined by the binomial rule $C_4^w(1-K)^{4-w}K^w$. In order to distinguish the TOF spectrum for collisions with one or two fragments from that for four fragments, four 1D multistop TOF spectra have been recorded (not presented here). They correspond to collision events where *w* different fragments (or stops), $w=1$, 2, 3 or 4, are detected. Such spectra are noted as *S (w stop)*. The relative intensity of a given fragment C_m^+ in a *w stop* spectrum is

$$A_w=\frac{w}{4}C_4^w(1-K)^{4-w}K^w.$$

The *3 stop* and *4 stop* spectra consist of only C_m^+ peaks with relative intensities A_3 and A_4, respectively. A C_{60-2n}^{4+}

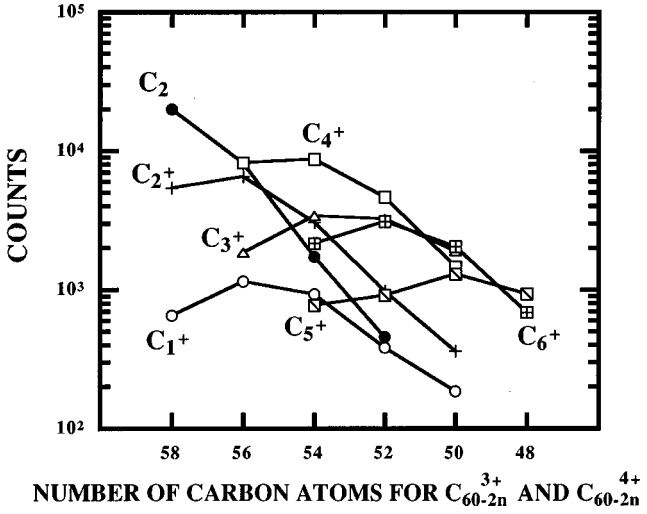

FIG. 5. Experimental abundance of fission and evaporation channels from a C_{60}^{4+} parent ion. For fission channels, $C_{60}^{4+}\rightarrow C_{60-2n}^{3+}+C_m^+$ ($m=1$, 2, 3, 4, 5, and 6), the small singly charged fragment is presented by different symbols. Solid circles present the abundance of evaporation channels, $C_{60}^{4+}\rightarrow C_{60-2n}^{4+}+n\ C_2$. The number of carbon atoms of the triply or quadruply charged heavy fragment for each channel is plotted along the *X* axis.

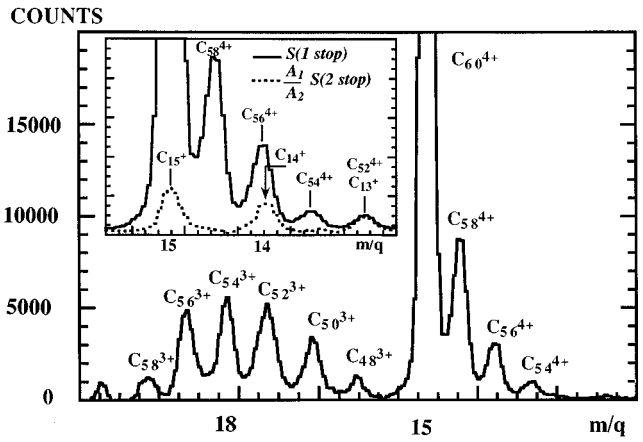

FIG. 6. Corrected C_{60-2n}^{4+} and C_{60-2n}^{3+} distribution. The inset shows the part of TOF spectrum corresponding to heavy C_{60-2n}^{4+} and medium mass C_{13}^{+}, C_{14}^{+}, and C_{15}^{+} peaks. The solid line represents a *1 stop* spectrum and the dotted line represents the scaled *3 stop* spectrum which has to be subtracted from the previous one to give the corrected intensities of the C_{60-2n}^{4+} peaks. The *X* axes are labeled in m/q where m is the number of carbon atoms of a fragment and q is the charge.

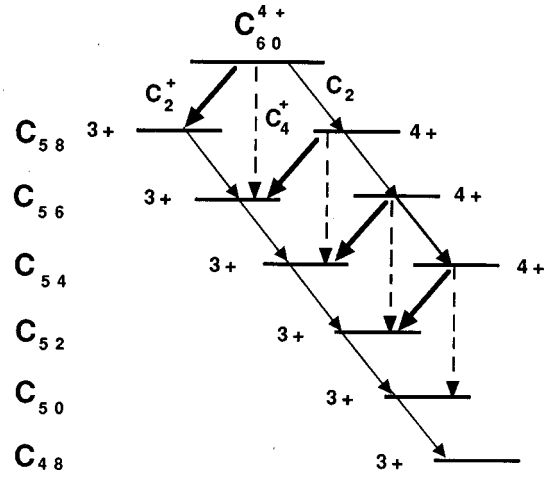

FIG. 7. Simplified dissociation scheme of a C_{60}^{4+} parent ion. A C_{60-2n}^{4+} precursory ion ($n=0,1,2\ldots$) has three decay channels with the loss of one C_2 (thin line arrow), one C_2^{+} (thick line arrow), or one C_4^{+} (broken line arrow) unit, respectively. A C_{60-2n}^{3+} precursory ion ($n=1,2,3\ldots$) has only one decay channel with the loss of one C_2 (thin line arrow) unit.

peak can be found only in the *1 stop* spectrum. It is probably mixed with a C_m^{+} peak with relative intensity A_1. The correction is thus made as follows:

$$S(1\ \ stop)-\frac{A_1}{A_3}(3\ \ stop)\quad (\text{see inset of Fig. 6}).$$

To normalize the data obtained from the 1D and 2D spectra, the intensities of the C_{60-2n}^{3+} peaks have to be measured. Such a peak can be found in both the *1 stop* and *2 stop* spectra. The correction for contribution of the C_m^{+} peaks is applied to the C_{60-2n}^{3+} spectrum:

$$S(1\ \ stop)-\frac{A_1}{A_3}(3\ \ stop)+S(2\ \ stop)-\frac{A_2}{A_3}(3\ \ stop).$$

The corrected evaporation C_{60-2n}^{4+} and fission C_{60-2n}^{3+} spectra are superimposed to give a total spectrum (Fig. 6). In our experiment, the detection probability K of medium mass singly charged ion is approximately 0.4. The importance of the correction is shown by the large difference between the partial populations of the C_{60-2n}^{4+} peaks without and with correction. Values of 0.46, 0.34, 0.08, and 0.11 are obtained from direct measurement [Fig. 3(c)] for $n=1$, 2, 3, and 4, respectively. These values become 0.66, 0.27, 0.06, and 0.01 after the correction.

IV. SIMULATION OF THE FRAGMENTATION SCHEME

A. Fragmentation scheme

A C_{60}^{4+} parent ion with an initial energy E^* can eject a small neutral or charged fragment by consuming at least a critical energy D and becomes a cooled heavy fragment with internal energy at most E^*-D. If this energy is not high enough for further dissociation, the heavy fragment remains stable. Corresponding to this case, populations of one-step dissociation such as $C_{60}^{4+}\rightarrow C_{58}^{4+}+C_2$, $C_{58}^{3+}+C_2^{+}$, $C_{56}^{3+}+C_4^{+}$, and $C_{54}^{3+}+C_6^{+}$ are observed. In other cases, if the remaining energy is still sufficient, other small fragments can be ejected. The C_{60-2n}^{4+} populations are the consequence of multistep evaporation, i.e., sequential losses of n C_2 neutral fragments. The direct loss of a C_4 unit will not be considered here, because it is negligible [8]. The decay scheme is more complicated for fission channels involving the emission of a small charged fragment. The later one could carry off enough internal energy for further dissociation. According to earlier studies on small carbon clusters [22], the monocharged ions C_6^{+}, C_5^{+}, C_4^{+}, C_3^{+}, and C_2^{+} decay preferentially to $C_3^{+}+C_3$, $C_3^{+}+C_2$, $C^{+}+C_3$, $C^{+}+C_2$, and $C^{+}+C$, respectively. Thus we can consider the measured small even-mass fragments C_2^{+}, C_4^{+}, and C_6^{+} as produced from direct asymmetrical dissociation of a charged fullerene, while the small odd-mass charged fragments can be attributed to a secondary dissociation process, such as $C_2^{+}\rightarrow C^{+}+C$, $C_4^{+}\rightarrow C^{+}+C_3$, and $C_6^{+}\rightarrow C_3^{+}+C_3$. With this analysis however, one can not explain the populations of $C_{56}^{3+}+C_3^{+}+C$ and $C_{54}^{3+}+C_5^{+}+C$, as the $C_4^{+}\rightarrow C_3^{+}+C$ and $C_6^{+}\rightarrow C_5^{+}+C$ channels are relatively weak. These populations can be thus considered as the result of simultaneous emission of two small fragments C_3^{+} and C or C_5^{+} and C from a charged fullerene.

To perform a simulation of the experimental results, the decay scheme is simplified. The fission channels producing C_3^{+} and C are associated with those of C_4^{+} and the fission channels producing C^{+} and C are associated with those of C_2^{+}. The processes leading to C_5^{+} and C_6^{+} ions, which represent 20% of the total fission population, are neglected. Notice that the resulting populations of $C_{60-2n}^{3+}+C_4^{+}$ ($n\geqslant 3$) are slightly overestimated, because part of $C_{60-2n}^{3+}+C_3^{+}$ ($n\geqslant 3$) population is contributed by the fragmentation of C_6^{+}. This deviation becomes more important as the mass of the heavy fragments decreases.

The simplified decay scheme of a C_{60}^{4+} consists of sequential losses of n C_2 or $(n-1)$ $C_2+C_2^{+}$ or $(n-2)$ $C_2+C_4^{+}$ (Fig. 7). From a C_{60-2n}^{4+} ($n=0,1\ldots$), three

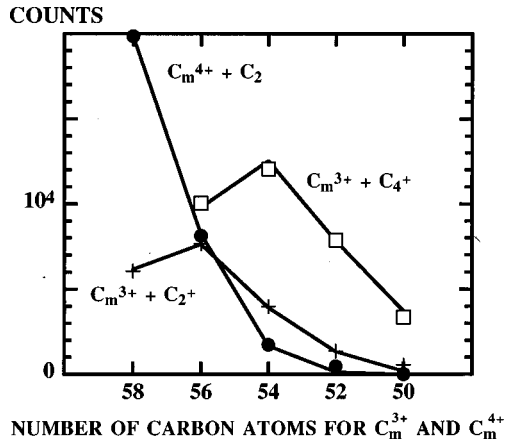

FIG. 8. Experimental abundance of dissociation channels leading to different final states, (+) $C_m{}^{3+}+C_2{}^+$ ($m\leqslant 58$), (□) $C_m{}^{3+}+C_4{}^+$ ($m\leqslant 56$), and (●) $C_m{}^{4+}+nC_2$ ($m\leqslant 58$). The number of carbon atoms of the triply or quadruply charged heavy fragment for each channel is plotted along the *X* axis. Full lines: reproduction of the experimental points with the RRK theory and the multistep cascade model.

asymmetrical decay channels are possible producing $C_{60-2(n+1)}{}^{4+}+C_2$, $C_{60-2(n+1)}{}^{3+}+C_2{}^+$, and $C_{60-2(n+2)}{}^{3+}+C_4{}^+$. The dissociation rate associated to each channel is noted as $A_{60-2n}{}^{4+}(C_2)$, $A_{60-2n}{}^{4+}(C_2{}^+)$, and $A_{60-2n}{}^{4+}(C_2{}^+)$, respectively. For $C_{60-2n}{}^{3+}$ ($n=1,2\ldots$), only the evaporation channel is considered with a dissociation rate $A_{60-2n}{}^{3+}(C_2)$, because the asymmetrical fission channel is negligible, as shown by the weak intensity of $C_m{}^{2+}$ peaks in Fig. 3(c). The measured population distribution for each state of the dissociation scheme is shown in Fig. 8.

B. Multistep cascade decay

The time-dependent population of a $C_{60-2n}{}^{4+}$ ion can be calculated by resolving the $n+1$ population equations associated to all involved intermediate states $C_{60}{}^{4+}\rightarrow\cdots C_{60-2k}{}^{4+}\rightarrow\cdots\rightarrow C_{60-2n}{}^{4+}$. The obtained result is

$$P_n=\prod_{k=0}^{n-1}A_k'\times\sum_{k=0}^{n}\frac{e^{-A_k t}}{\Pi_{j=0,j\neq k}^{n}(A_k-A_j)}, \tag{1}$$

where A_k and A_k' are the total and partial dissociation rates of $C_{60-2k}{}^{4+}$. Here, $A_k'=A_{60-2k}{}^{4+}(C_2)$, $A_k=A_{60-2k}{}^{4+}(C_2)+A_{60-2k}{}^{4+}(C_2{}^+)+A_{60-2k}{}^{4+}(C_4{}^+)$.

The population of $C_{60-2n}{}^{3+}+C_2{}^+$ is produced by *n-step* sequential losses of $(n-1)$ C_2 and a $C_2{}^+$. To reach this state, *n* different channels are possible with the emission of $C_2{}^+$ unit at the first, second,..., or, last step. The population contributed by each channel is noted by $P_{n,i}$, where *i* labels the step for the loss of $C_2{}^+$ in a cascade such as $C_{60}{}^{4+}\rightarrow\cdots C_{60-2(i-1)}{}^{4+}\rightarrow C_{60-2i}{}^{3+}\rightarrow\cdots\rightarrow C_{60-2n}{}^{3+}$. The final population is obtained by the summation $\Sigma_{i=1}^{n}P_{n,i}$. The $P_{n,i}$ values are calculated using Eq. (1). For $k\leqslant i-1$, the total dissociation rate A_k of a $C_{60-2k}{}^{4+}$ state is calculated in the same way as in the case of the evaporation channel. For $k\geqslant i$, A_k equals $A_{60-2k}{}^{3+}(C_2)$. For $k<i-1$, $k=i-1$, and $k\geqslant i$, the partial dissociation rate A_k' is $A_{60-2k}{}^{4+}(C_2)$; $A_{60-2k}{}^{4+}(C_2{}^+)$, and $A_{60-2k}{}^{3+}(C_2)$, respectively. For a $C_{60-2n}{}^{3+}+C_4{}^+$ channel the population is calculated in a similar way.

C. Dissociation rate

The dissociation rate for a channel from a precursory ion $C_m{}^{q+}$ is calculated using the simple RRK theory, initially developed by Rice, Ramsperger, and Kassel [19,20] to interpret the unimolecular dissociation of molecules. This model has been recently applied to clusters [23,24]. The internal energy E^* of a $C_m{}^{q+}$ ion is statistically distributed among the $3m-6$ vibrational modes considered as a collection of independent harmonic oscillators with vibrational frequency ν_0. A dissociation occurs only if a critical energy *D* is accumulated in at least one oscillator. The reaction rate constant $A(E^*)$ is thus given by

$$A(E^*)=n_s\nu_0\left(1-\frac{D}{E^*}\right)^{3m-7}, \tag{2}$$

where n_s, the degeneracy factor, is the number of atoms on the surface of a C_m fullerene, $n_s=m$; and $\nu_0=2.7\times10^{13}\,s^{-1}$ is the Debye frequency of C_{60} [25], which characterizes the energy redistribution rate. After an asymmetrical dissociation process, the remaining internal energy E^*-D is in principle distributed statistically among all the oscillators. However, in a first approximation, we consider that all this energy is carried off by the heavy fragment for further possible dissociation processes.

The critical energy for evaporation is considered as the dissociation energy of a C_2 unit from a $C_m{}^+$ fullerene. The values have been estimated by Wörgötter *et al.* for $50\leqslant m\leqslant 60$ [18] and noted as D_m. For fission channels, the critical energy is described as the Coulomb fission barrier height from the simple liquid-drop model and noted as $B_m(C_2{}^+)$ and $B_m(C_4{}^+)$ for the loss of a $C_2{}^+$ and a $C_4{}^+$ from a $C_m{}^{4+}$ fullerene, respectively.

D. Simulation

The multistep cascade decay model is used to calculate the population distribution on $C_{60-2n}{}^{4+}$, $C_{60-2n}{}^{3+}+C_2{}^+$, and $C_{60-2n}{}^{3+}+C_4{}^+$ states 250 ns after each collision. This delay, referred as $t_{\max}$, is the flight time of a $C_{60}{}^{4+}$ in the extraction field. It corresponds to the time range for observing delayed dissociation processes in our experiments. The fission barriers $B_m(C_2{}^+)$, $B_m(C_4{}^+)$ and the initial energy E^* of the parent $C_{60}{}^{4+}$ fullerene are adjusted to reproduce the measured population distribution. A good agreement between the calculation and the experimental data has been obtained (Fig. 8). The initial energy profile of the $C_{60}{}^{4+}$ has been assumed to be a Gaussian distribution centered at 65 eV with a total width of 12 eV. The obtained fission barriers, $B_m(C_2{}^+)$ and $B_m(C_4{}^+)$, are shown in Fig. 9.

For the parent ion $C_{60}{}^{4+}$, the critical energies associated to the three competing channels, $C_{60}{}^{4+}\rightarrow C_{58}{}^{4+}+C_2$, $C_{56}{}^{3+}+C_4{}^+$ and $C_{58}{}^{3+}+C_2{}^+$ are found to verify the relation $D_{60}<B_{60}(C_4{}^+)<B_{60}(C_2{}^+)$. When the mass of a fullerene becomes smaller, the fission barrier $B_m(C_2{}^+)$ decreases

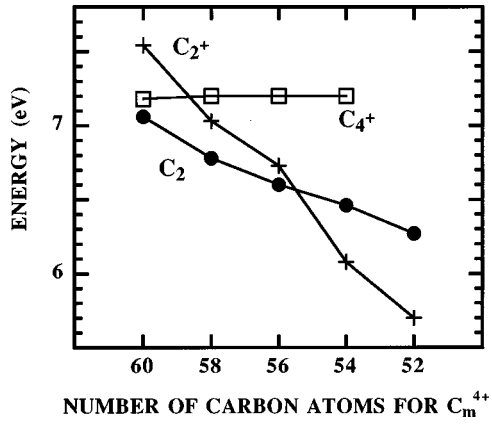

FIG. 9. Dissociation energies as a function of the number of carbon atoms of the precursory ion C_m^{4+}. (●) $D_m(C_2)$ from Ref. [18]. (+) $B_m(C_2^+)$, with error bar 0.1 eV and (□) $B_m(C_4^+)$, adjusted values obtained in the dissociation scheme simulation.

slowly to become lower than the evaporation energy D_m for m smaller than 56. A critical size $n_c=56$ can be thus defined for quadruply charged fullerene C_m^{4+}. For large size, $m>n_c$, the fission barrier $B_m(C_2^+)$ is higher than the evaporation energy D_m. The evaporation channel predominates in this case. For the critical size, $m\simeq n_c$, and then $D_m\simeq B_m(C_2^+)$, the evaporation and fission channels have the same probability. For small size, $m<n_c$, $D_m>B_m(C_2^+)$, the fission channel prevails. The similar size dependence has been observed in charged metallic clusters [26]. The uncertainty of the $B_m(C_2^+)$ values is approximately 0.1 eV. The fission barriers $B_m(C_4^+)$ are reliable for $m=60$ and 58. They are unprecise for $m\leqslant 56$, because of the relatively important contribution of the C_6^+ fission channel to the $C_m^{3+}+C_3^+$ populations for $m\leqslant 52$.

V. ANALYSIS OF ''SLOW'' AND ''FAST'' FISSION PROCESSES

In a multistep cascade process, the dissociation rate of the last decay step is much lower than those of the previous steps, because its precursory ion is less energetic. A simple example is given by the two-step decay channels with successive losses of C_2^+ and C_2 or C_2 and C_2^+ leading to the $C_{56}^{3+}+C_2^+$ population. The dissociation rate is much higher if the C_2^+ is lost at the first step than if it is lost at the last step. These two channels are then characterized by a ''fast fission'' process and a ''slow fission'' process. In our model, the contribution of the slow fission to the total $C_{56}^{3+}+C_2^+$ population is calculated to be approximately 60%. In a similar way, for the $C_{54}^{3+}+C_2^+$ population, approximately 40% of the simulated population is due to the slow fission channel with successive losses of C_2, C_2, and C_2^+.

On the other hand, in our experiments, it is possible to distinguish populations produced from slow fission or from fast fission. In a fast fission process, the small charged fragment is rapidly lost in the collision region. In a slow fission process, it is lost in the extraction field with a delay. In the 2D-fragment correlation spectrum (Fig. 4), a slow fission process is identified by the long oblique tail that enlarges a spot towards smaller TOF for the heavy fragment and towards larger TOF for the small fragment. The slopes of the

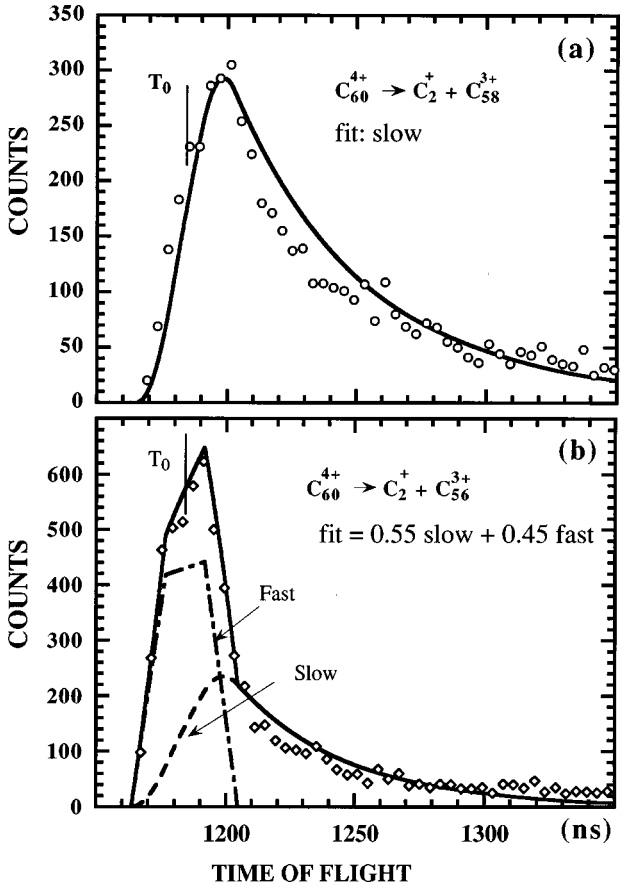

FIG. 10. The Y projections of the $C_2^+ + C_{58}^{3+}$ and $C_2^+ + C_{56}^{3+}$ spots of the correlated recoil ion 2D spectrum (Fig. 4) giving the measured differential population intensities. They are shown by circles and diamonds as a function of the flight time of the C_2^+ fragment. T_0 is the time of flight of a C_2^+ fragment produced in a nondelayed fission event. Slow curve (a,b): an exponential curve, $\exp\{-[(T-T_0)/50\ \text{ns}]\}$, convoluted by a broadening function, that takes the initial velocity distribution due to the Coulomb repulsion and the instrumental width into account. Fast curve (b): a function $\delta(T-T_0)$ convoluted by the same broadening function as in the case of the slow curve. Full lines of (a) and (b): linear combinations of the fast and slow curves for fitting the experimental points. (a) 100% of slow; (b) about 55% of slow.

resulting tails are well reproduced by a calculation taking into account the delayed fission.

The vertical projection of the $C_{58}^{3+}+C_2^+$ spot [Fig. 10(a)] shows the differential population I for this channel as a function of the time of flight T of the C_2^+ fragment. The experimental curve is fitted by an exponential decay function $e^{-[(T-T_0)/\tau]}$ with a characteristic time $\tau=50$ ns, where T_0 is the time of flight of a C_2^+ produced immediately after the collision. The maximum of the curve is shifted from T_0 because of two broadening factors. The first one is the C_2^+ initial velocity distribution due to the Coulomb repulsion between the two charged fragments leading to a total width of about 28 ns in the time of flight. The second one is the instrumental width, which is approximately 13 ns. To interpret this measured exponential decay, we write the differential population $I(T)$ for the $C_{58}^{3+}+C_2^+$ channel on the following form:

$$I(T)=\int \frac{dP(C_{58}{}^{3+}+C_2{}^{+},E^*)}{dT}dE^* = \int A_{60\to 58}P_{60}(E^*)e^{-A_{58}t_{\max}}e^{-(A_{60}-A_{58})t}\frac{dt}{dT}dE^*, \quad (3)$$

where A_{60} and A_{58} are the total dissociation rates for $C_{60}{}^{4+}$ and $C_{58}{}^{3+}$, $A_{60\to 58}$ is the partial dissociation rate of the channel $C_{60}{}^{4+}\to C_{58}{}^{3+}+C_2{}^{+}$, and $P_{60}(E^*)$ is the energy distribution of the initial $C_{60}{}^{4+}$ population. Note that this formula gives the population of $C_{58}{}^{3+}+C_2{}^{+}$ produced with a delay t and in addition the $C_{58}{}^{3+}$ ion stays stable until $t_{\max}$. The dependence of the flight time T of $C_2{}^{+}$ on the delayed fission time t is found to be a fourth-order polynomial. For small t values, the delay time t is approximated as $T-T_0$. The measured characteristic time of 50 ns gives in fact a measurement of the average value $1/(A_{60}-A_{58})$. On the other hand, the rates A_{60}, A_{58}, and $A_{60\to 58}$ can be calculated as a function of the energy E^* with Eq. (2). For an initial energy of $E^*=68$ eV, the coefficient $A_{60\to 58}P_{60}(E^*)e^{-A_{58}t_{\max}}$ is maximum. This determines the most probable value of $1/(A_{60}-A_{58})$ to be approximately 65 ns. The agreement between the theoretical and the experimental values is satisfactory.

The vertical projection of the $C_{56}{}^{3+}+C_2{}^{+}$ spot is shown in Fig. 10(b). It is the superposition of two curves. The ''slow'' curve, obtained in the same way as for the case of $C_{58}{}^{3+}+C_2{}^{+}$, corresponds to the successive losses of C_2 and $C_2{}^{+}$. The ''fast'' curve presents the differential population distribution of $C_2{}^{+}$ ions with the flight time T_0 taken into account for the two broadening factors. It is associated to the successive losses of $C_2{}^{+}$ and C_2. The slow fission population is found to be 55% of the total population. Similar analysis has been performed for the $C_{54}{}^{3+}+C_2{}^{+}$ spot. The contribution of the slow fission is found to be 35%. These results are in good agreement with the simulation calculation which gives a slow fission contribution of 60% and 40% in these two cases. This comparison allows us to justify the validity of our model.

VI. CONCLUSION

The decay scheme of the multicharged fullerene ion $C_{60}{}^{4+}$ has been studied in a time range of approximately 250 ns. The partial populations of asymmetrical fission and evaporation channels have been measured. The experimental data have been reproduced using the RRK theory and the multistep cascade model. The initial energy of the parent ion is estimated to approximately 65 eV. The dissociation energies are evaluated for the asymmetrical fission channels, $C_m{}^{4+}\to C_{m-2}{}^{3+}+C_2{}^{+}$ and $C_m{}^{4+}\to C_{m-4}{}^{3+}+C_4{}^{+}$ ($m=60,58,56,54$). A critical size of the quadruply charged fullerenes $C_m{}^{4+}$ is found to be around $m=56$. For this size, the evaporation by loss of a C_2 dimer and the fission by loss of a $C_2{}^{+}$ ion are equally probable. The validity of our model is justified by a detailed analysis of the 2D fragment correlation spectrum giving further information on the fast and slow fission processes. For the dissociation processes studied in this work, the internal energy of the parent $C_{60}{}^{4+}$ ions is evaluated to be about three times the energy of the giant dipole plasmon resonance in a C_{60} molecule. The collective excitation of the valence electrons in such a resonance is used to interpret the energy transfer in photon excitation and in high-energy large-impact-parameter collisions [1,2,3,10]. However, for low-energy multicharged ion-C_{60} collisions, no conclusive argument on the possible resonance process concerning the excitation mechanism of the C_{60} fullerene can be obtained from the present measurements.

ACKNOWLEDGMENT

This work was supported by the Région Rhône-Alpes under Grant Nos. 97027-223 and 97027-283, of the Convention Recherche, Programme Emergence.

[1] I. V. Hertel, H. Steger, J. de Vries, B. Weisser, C. Menzel, B. Kamke, and W. Kamke, Phys. Rev. Lett. **68**, 784 (1992).
[2] S. Hunsche, T. Starczewski, A. L'Huillier, A. Persson, C.-G. Wahlström, B. Van Linden van den Heuvell, and S. Svanberg, Phys. Rev. Lett. **77**, 1966 (1996).
[3] S. Aksela, E. Nõmmiste, J. Jauhiainen, E. Kukk, J. Karvonen, H. G. Berry, S. L. Sorensen, and H. Aksela, Phys. Rev. Lett. **75**, 2112 (1995).
[4] C. Brink, L. H. Andersen, P. Hvelplund, and D. H. Yu, Z. Phys. D **29**, 45 (1994).
[5] P. Scheier and T. D. Märk, Phys. Rev. Lett. **73**, 54 (1994).
[6] P. Scheier, B. Dünser, and T. D. Märk, Phys. Rev. Lett. **74**, 3368 (1995).
[7] T. D. Märk and P. Scheier, Nucl. Instrum. Methods Phys. Res. B **98**, 469 (1995).
[8] P. Scheier, B. Dünser, R. Wörgötter, D. Muigg, S. Matt, O. Echt, M. Foltin, and T. D. Märk, Phys. Rev. Lett. **77**, 2654 (1996).
[9] B. Dünser, O. Echt, P. Scheier, and T. D. Märk, Phys. Rev. Lett. **79**, 3861 (1997).
[10] T. LeBrun, H. G. Berry, S. Cheng, R. W. Dunford, H. Esbensen, D. S. Gemmell, E. P. Kanter, and W. Bauer, Phys. Rev. Lett. **72**, 3965 (1994); S. Cheng, H. G. Berry, R. W. Dunford, H. Esbensen, D. S. Gemmell, E. P. Kanter, T. LeBrun, and W. Bauer, Phys. Rev. A **54**, 3182 (1996).
[11] B. Walch, C. L. Cocke, R. Voelpel, and E. Salzborn, Phys. Rev. Lett. **72**, 1439 (1994).
[12] Jian Jin, H. Khemliche, M. H. Prior, and Z. Xie, Phys. Rev. A **53**, 615 (1996).
[13] N. Selberg, A. Barany, C. Biedermann, C. J. Setterlind, H. Cederquist, A. Langereis, M. O. Larsson, A. Wännström, and P. Hvelplund, Phys. Rev. A **53**, 874 (1996).
[14] S. Martin, L. Chen, J. Bernard, A. Denis, and J. Désesquelles, Phys. Rev. A **59**, R1738 (1999).
[15] S. Martin, J. Bernard, L. Chen, A. Denis, and J. Désesquelles, Eur. Phys. J. D **4**, 1 (1998).

[16] S. Martin, L. Chen, J. Bernard, A. Denis, and J. Désesquelles, Phys. Rev. A **57**, 4518 (1998).
[17] M. Foltin, M. Lezius, P. Scheier, and T. D. Märk, J. Chem. Phys. **98**, 9624 (1993).
[18] R. Wörgötter, B. Dünser, P. Scheier, T. D. Märk, M. Foltin, C. E. Klots, J. Laskin, and C. Lifshitz, J. Chem. Phys. **104**, 1225 (1996).
[19] O. K. Rice and H. C. Ramsperger, J. Am. Chem. Soc. **49**, 1617 (1927).
[20] K. S. Kassel, J. Phys. Chem. **32**, 225 (1928).
[21] F. Aumayr, G. Lakits, and H. Winter, Appl. Surf. Sci. **47**, 139 (1991).
[22] K. Raghavachari and J. S. Binkley, J. Chem. Phys. **87**, 2191 (1987).
[23] C. Bréchignac, Ph. Cahuzac, F. Carlier, M. De Frutos, N. Kebaïli, J. Leygnier, A. Sarfati, and V. M. Akulin (unpublished).
[24] E. Cottancin, M. Pellarin, J. Lermé, B. Baguenard, B. Palpant, J. L. Vialle, and M. Broyer, J. Chem. Phys. **107**, 757 (1997).
[25] R. E. Santon and M. D. Newton, J. Phys. Chem. **92**, 2141 (1988).
[26] C. Bréchignac, Ph. Cahuzac, F. Carlier, and M. De Frutos, Nucl. Instrum. Methods Phys. Res. B **88**, 91 (1994).